Supporting Information

Flexible, Transparent Ion-conducting Membranes from Two-dimensional Nanoclays of Intrinsic Conductivity

Li Cao[a,b], Hong Wu[a,b,c], Xueyi He[a,b], Haobo Geng[a,b], Runnan Zhang[a,b], Ming Qiu[a,b], Pengfei Yang[a,b], Benbing Shi[a,b], Niaz Ali Khan[a,b], Zhongyi Jiang[a,b,d*]*

a Key Laboratory for Green Chemical Technology of Ministry of Education, School of Chemical Engineering and Technology, Tianjin University, Tianjin 300072, China

b Collaborative Innovation Center of Chemical Science and Engineering (Tianjin), Tianjin 300072, China

c Tianjin Key Laboratory of Membrane Science and Desalination Technology, Tianjin University, Tianjin 300072, China

d Joint School of National University of Singapore and Tianjin University, International Campus of Tianjin University, Binhai New City, Fuzhou, 350207, China

* Corresponding author:

e-mail: wuhong@tju.edu.cn; zhyjiang@tju.edu.cn

Fig. S1 A photo of thermally expanded vermiculite powders. The particle size of silvery white vermiculite powders is about 8-13 mm.

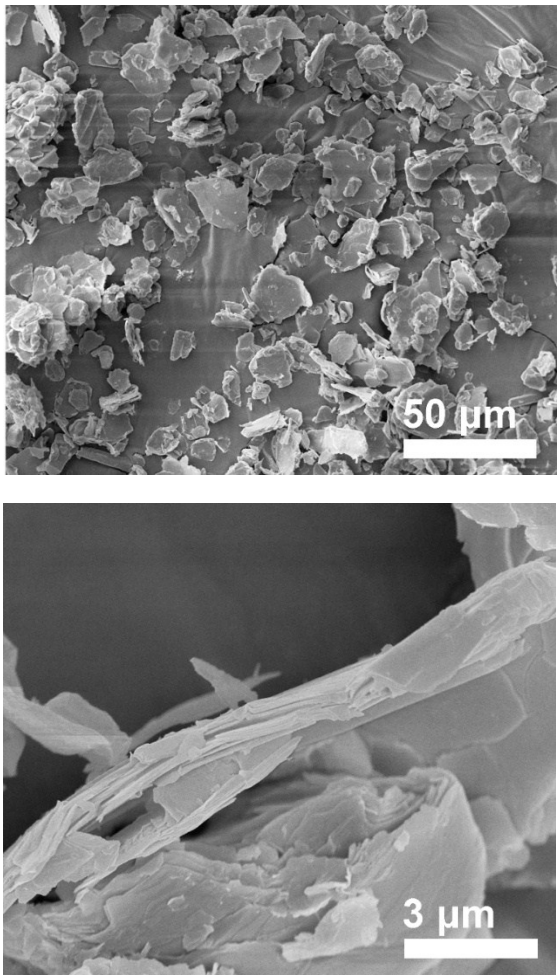

Fig. S2 SEM images of thermally expanded vermiculite powders. It shows layered-structure.

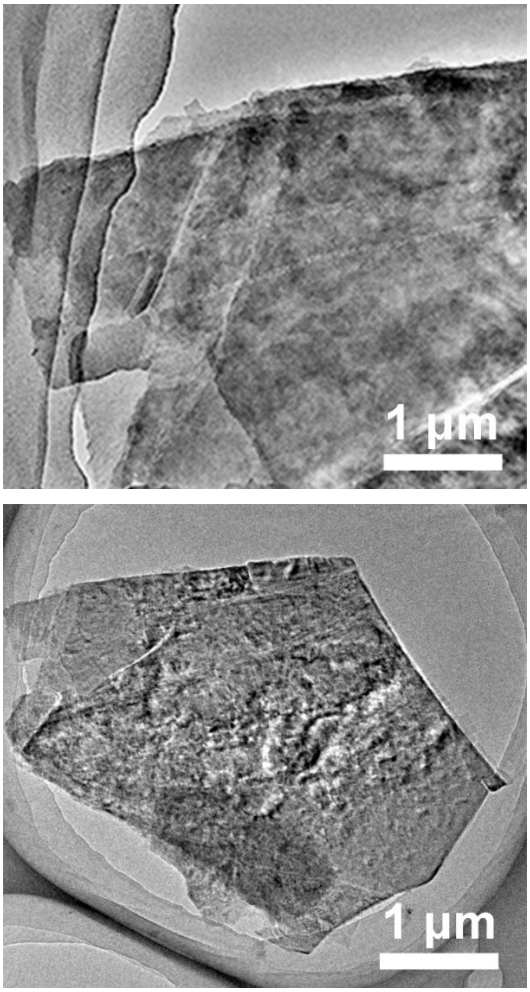

Fig. S3 TEM images of thermally expanded vermiculite powders.

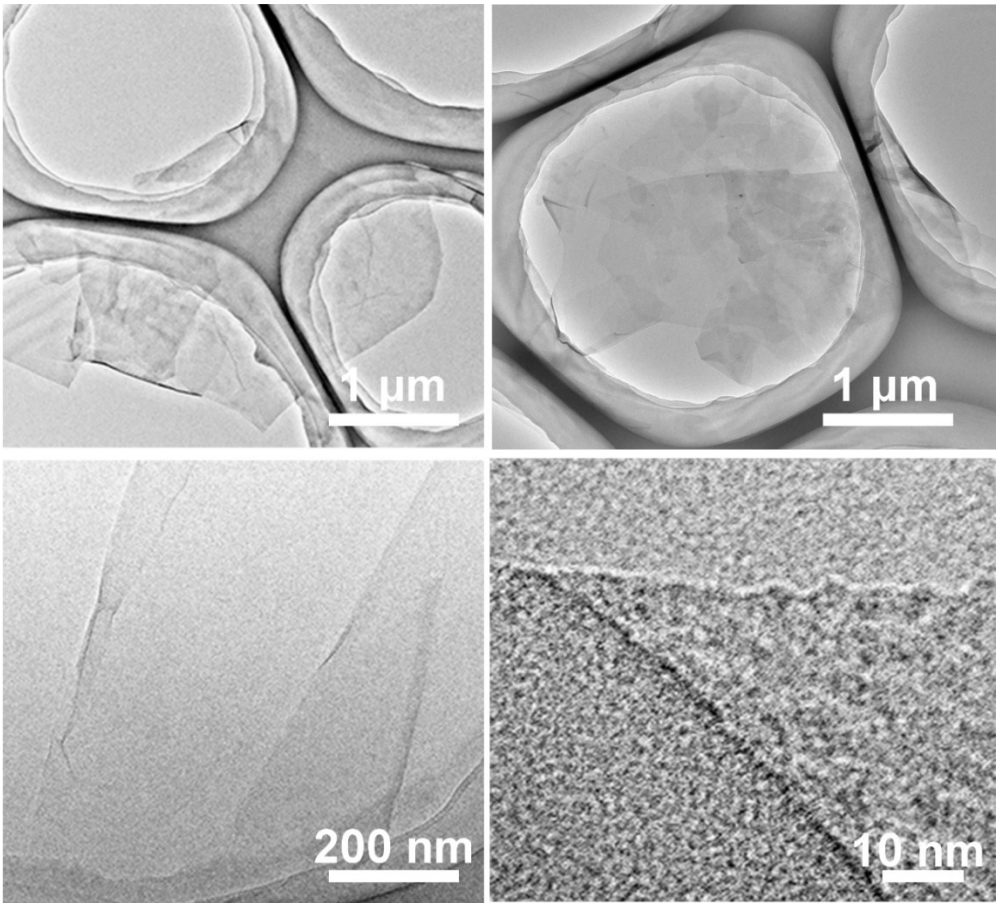

Fig. S4 TEM images of exfoliated vermiculite nanosheets.

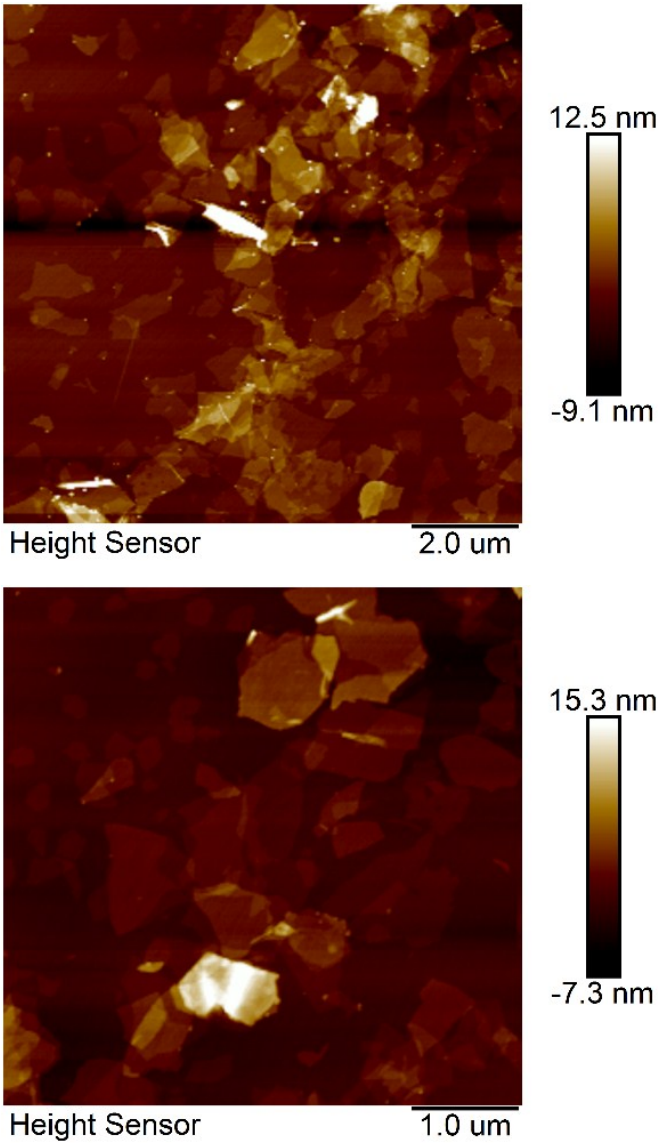

Fig. S5 AFM images of vermiculite nanosheets.

Fig. S6 A photo of vermiculite nanosheets suspensions after 25 months. A nearly transparent vermiculite nanosheets dispersion with a concentration of 1 mg mL^{-1} was obtained after removing the unexfoliated vermiculite flakes by centrifugation at 10000 r.p.m. for 20 min. The vermiculite nanosheets suspensions can keep stable and no appreciable precipitation was found even after 25 months.

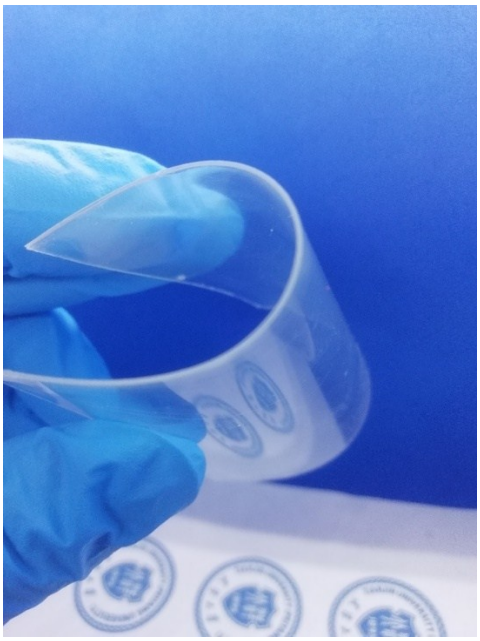

Fig. S7 A photo of vermiculite membrane on PET using a spray-coating method.

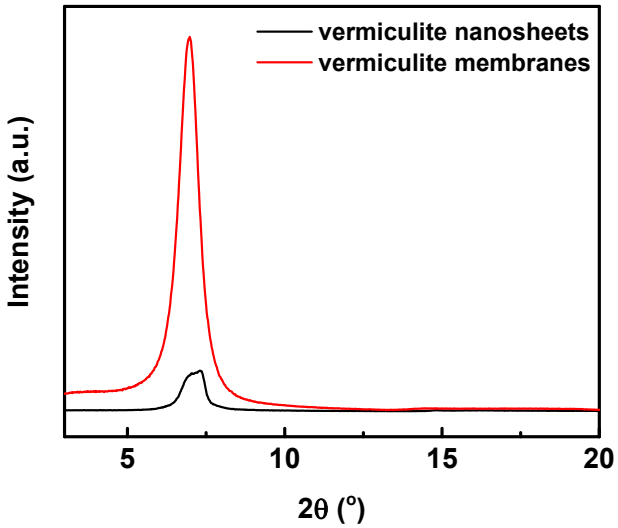

Fig. S8 XRD patterns of vermiculite nanosheets (black line) and vermiculite membranes (red line). the diffraction peak of vermiculite nanosheets at around 7° is weaker and broader compared to vermiculite membranes, indicating that the vermiculite nanosheets are less ordered stacked.

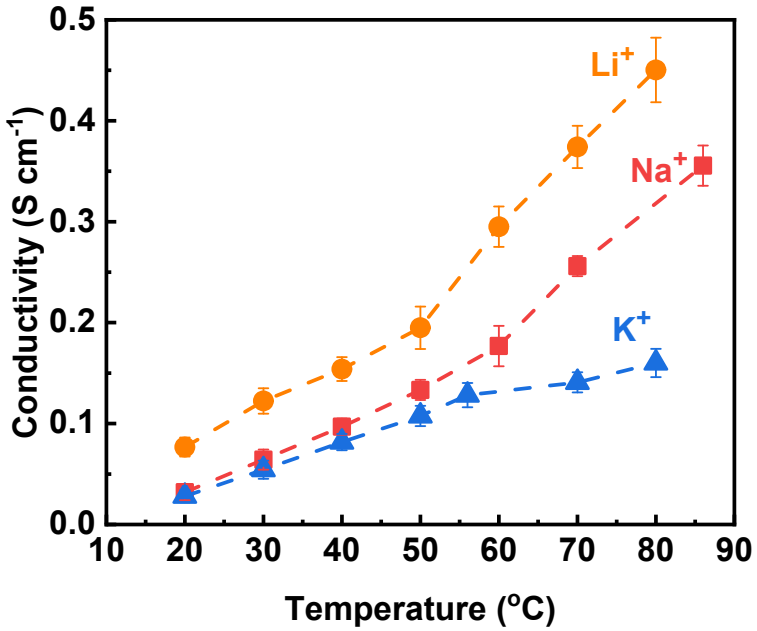

Fig. S9 Li^+, Na^+ and K^+ conductivity of vermiculite membranes as a function of temperature.

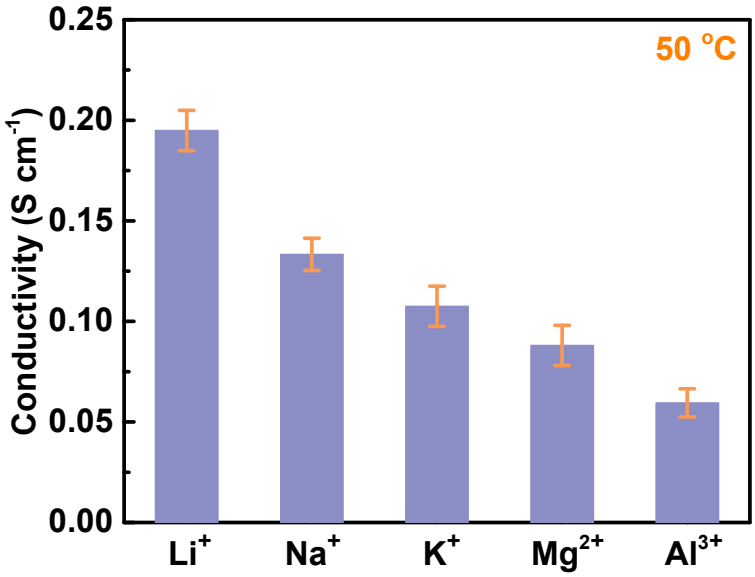

Fig. S10 Various cations (Li^+, Na^+, K^+ , Mg^{2+}, Al^{3+}) conductivities of vermiculite membranes at 50 °C.

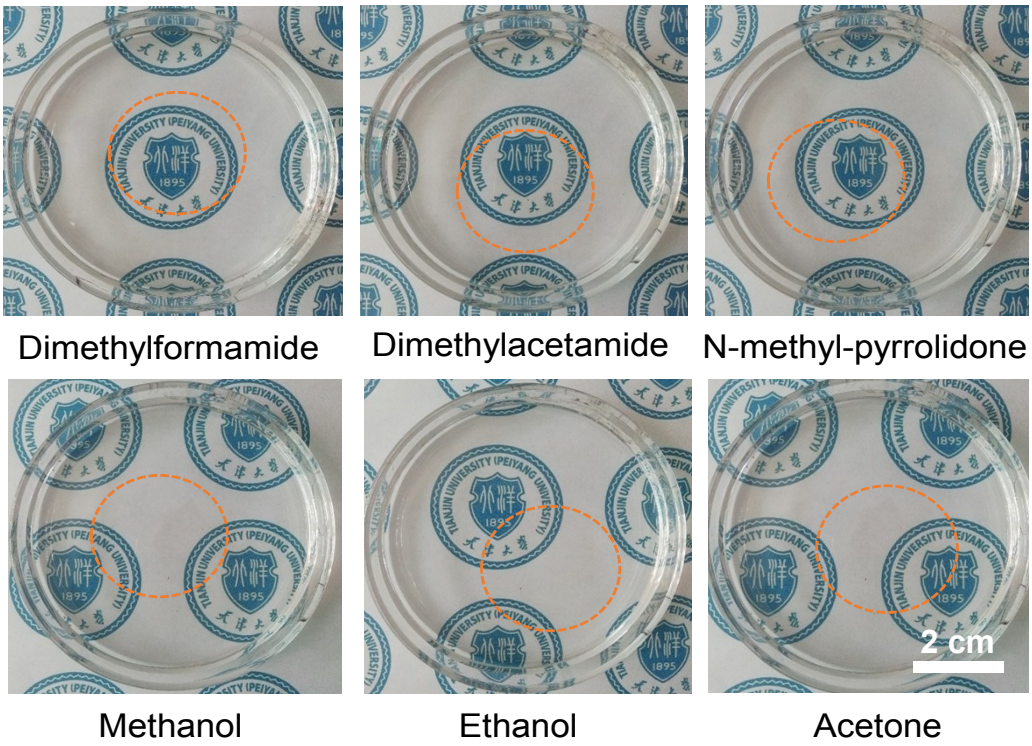

Fig. S11 Photos of vermiculite membranes in organic solvents. The vermiculite membranes are highly stable in varous organic solvents.

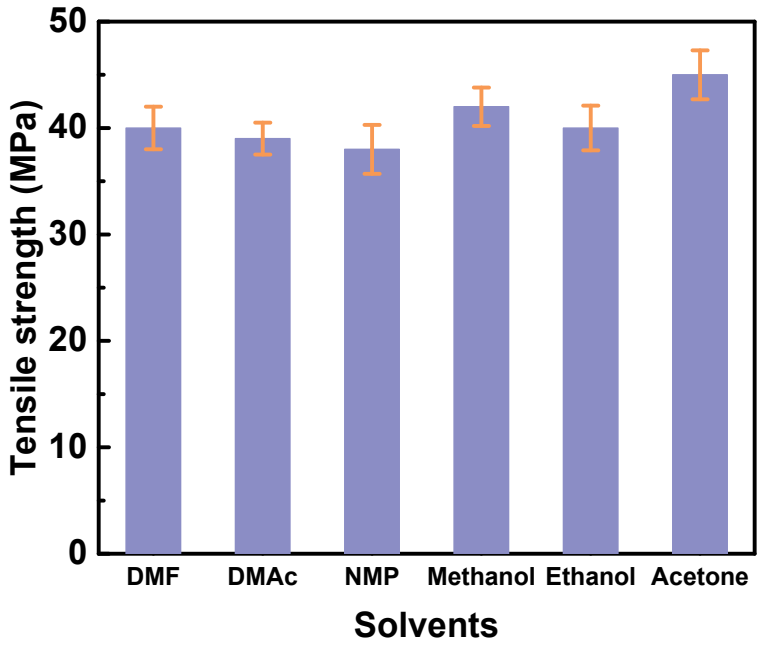

Fig. S12 Tensile strength of vermiculite membranes after storing in organic solvents for one week.

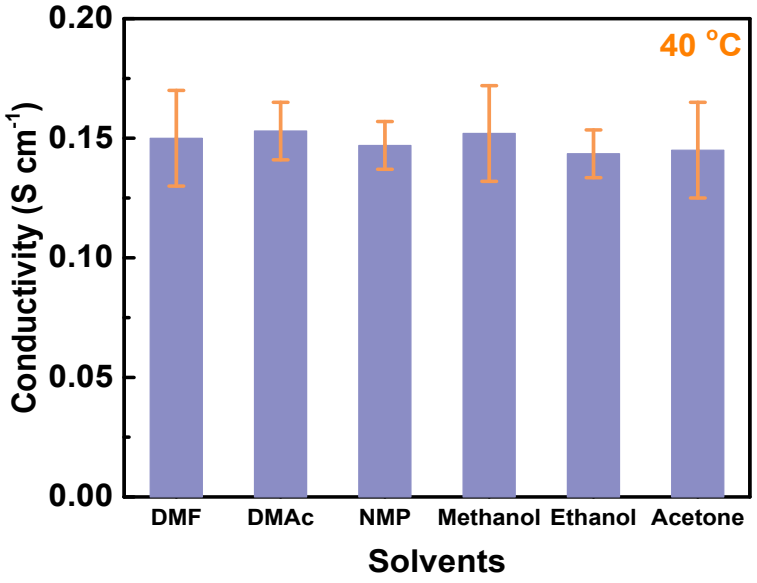

Fig. S13 Li^+ conductivity of vermiculite membranes after storing in organic solvents for one week.

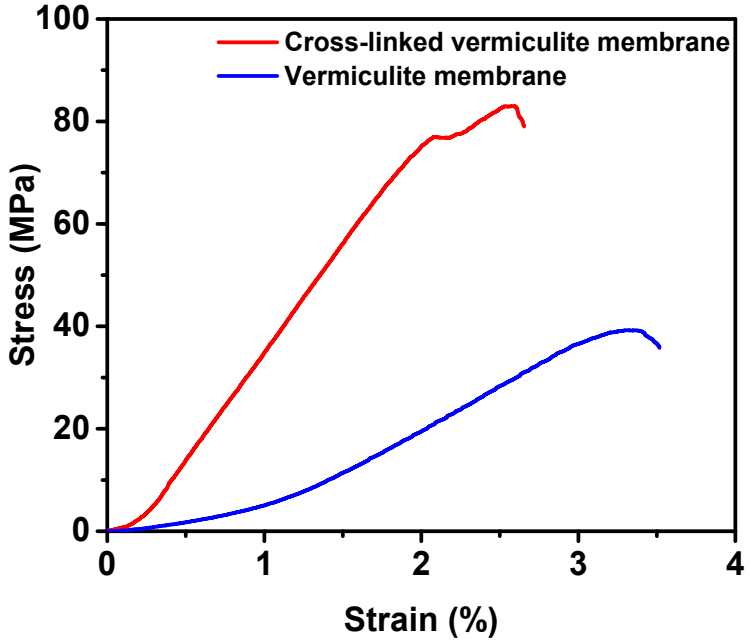

Fig. S14 Typical stress-strain curves of vermiculite membranes. Blue and red lines represent initial vermiculite membrane and cross-linked vermiculite membrane, respectively. After cross-linking with glutaraldehyde, the tensile strength of vermiculite membranes is twice as high as that of the pristine vermiculite membranes.

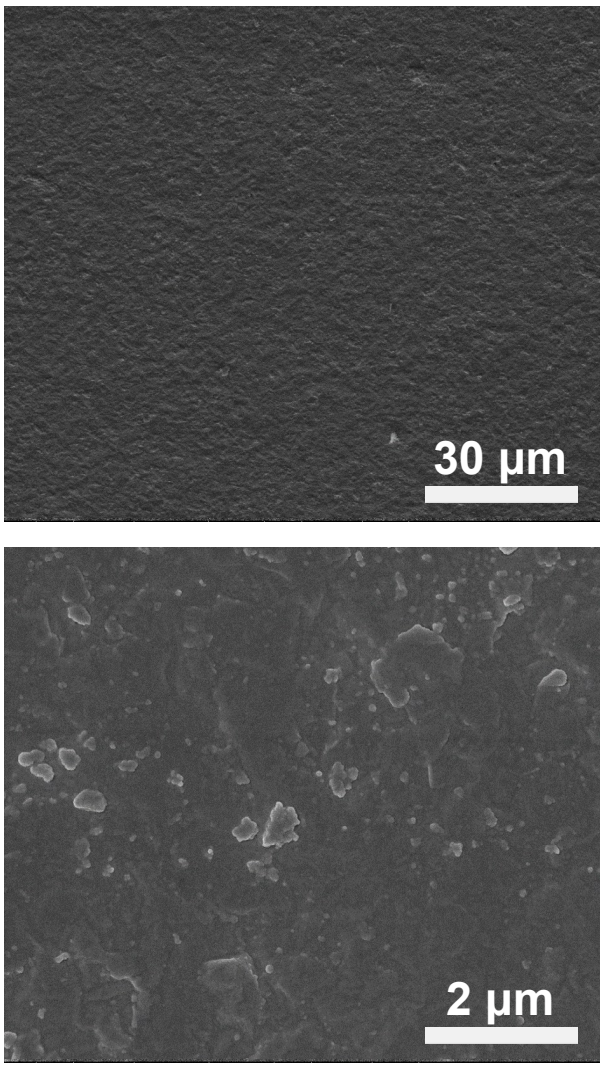

Fig. S15 Surface SEM images of vermiculite membranes after soaking in DMF at 100 ^{o}C for 24h.

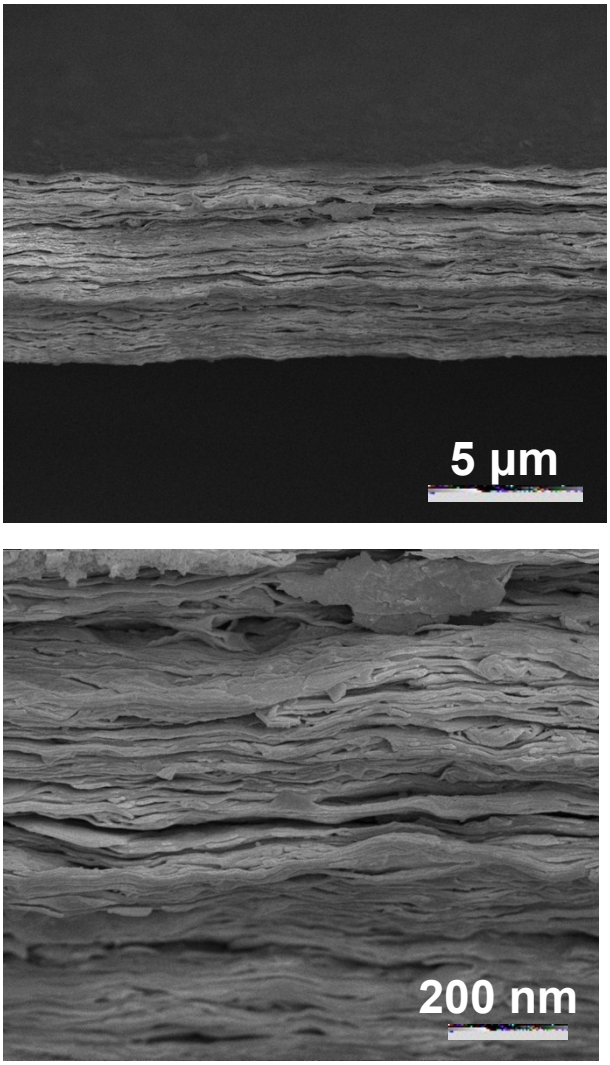

Fig. S16 Cross-section SEM images of vermiculite membrane after soaking in DMF at 100 ^{o}C for 24h.

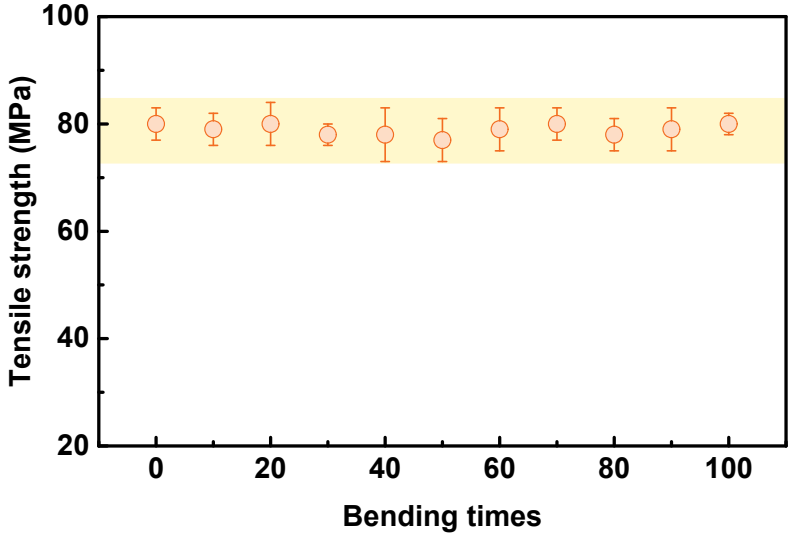

Fig. S17 Tensile strength of cross-linked vermiculite membranes during 100 bending tests.

Fig. S18 The cross-linked vermiculite membranes were attached to a hand, while completely maintaining structural integrity

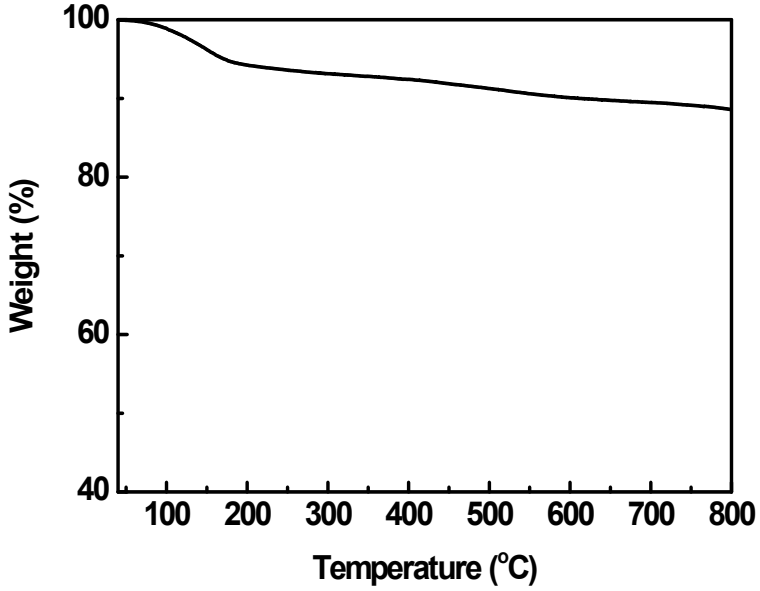

Fig. S19 TGA curve of vermiculite membranes.

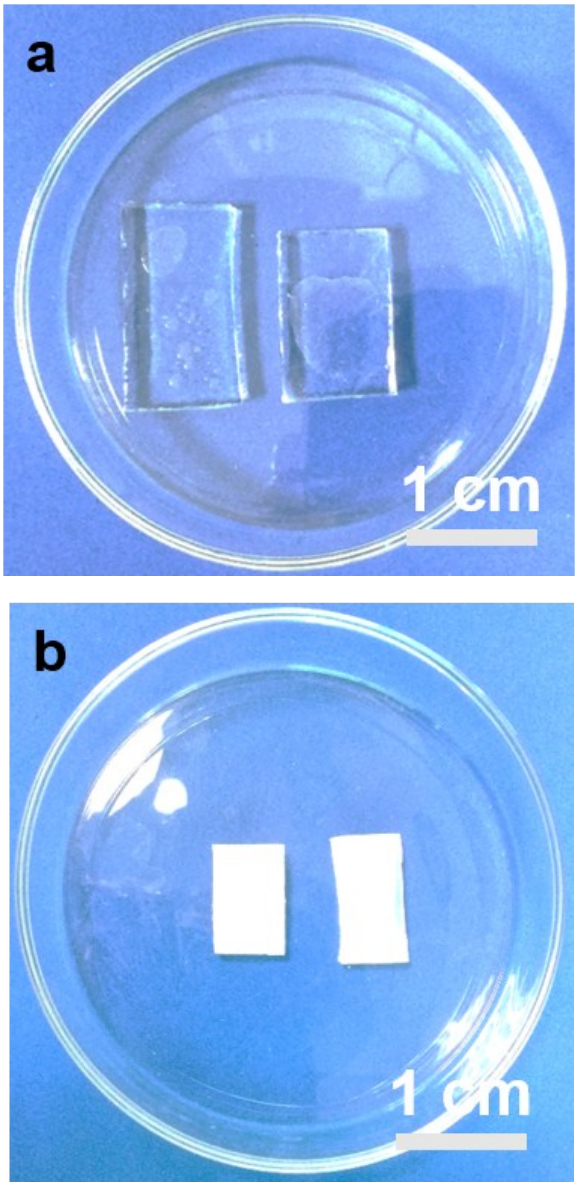

Fig. S20 Photos of initial conductive hydrogel (a) and dehydrated hydrogel (b). Compared with the initial hydrogel, the dehydrated hydrogel shows severe changes in both volume (shrinkage) and transparency (opaque).

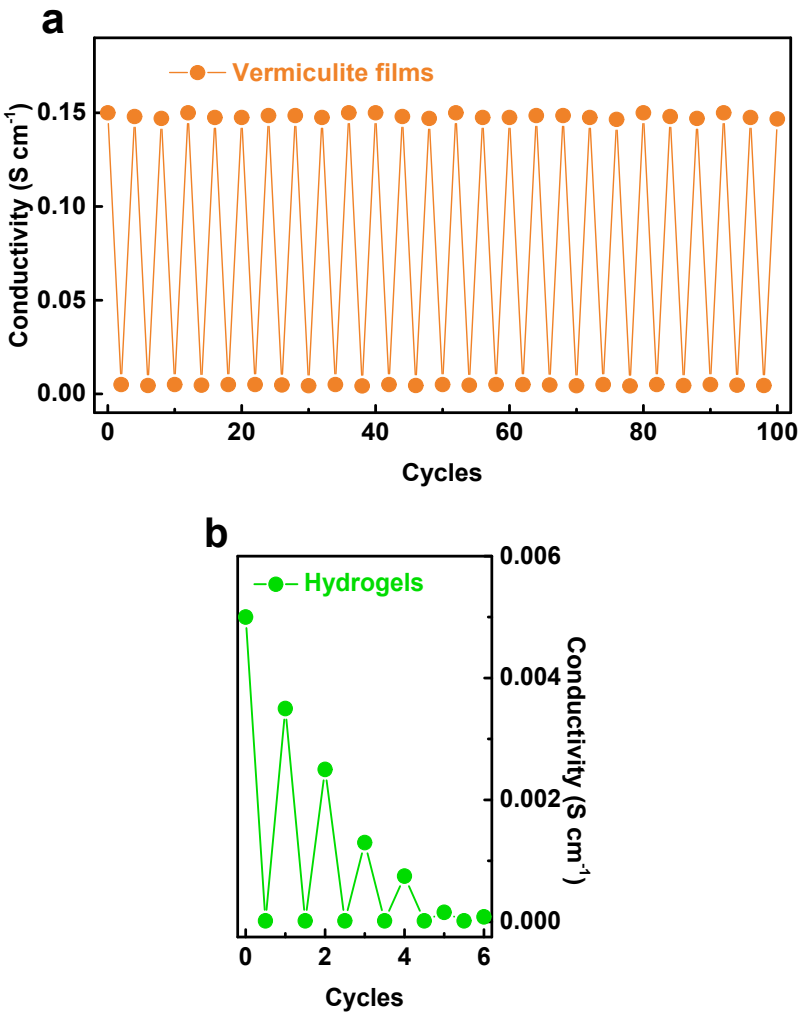

Fig. S21 Conductivity of vermiculite membranes (a) and hydrogels (b) during dehydration-hydration cycles.

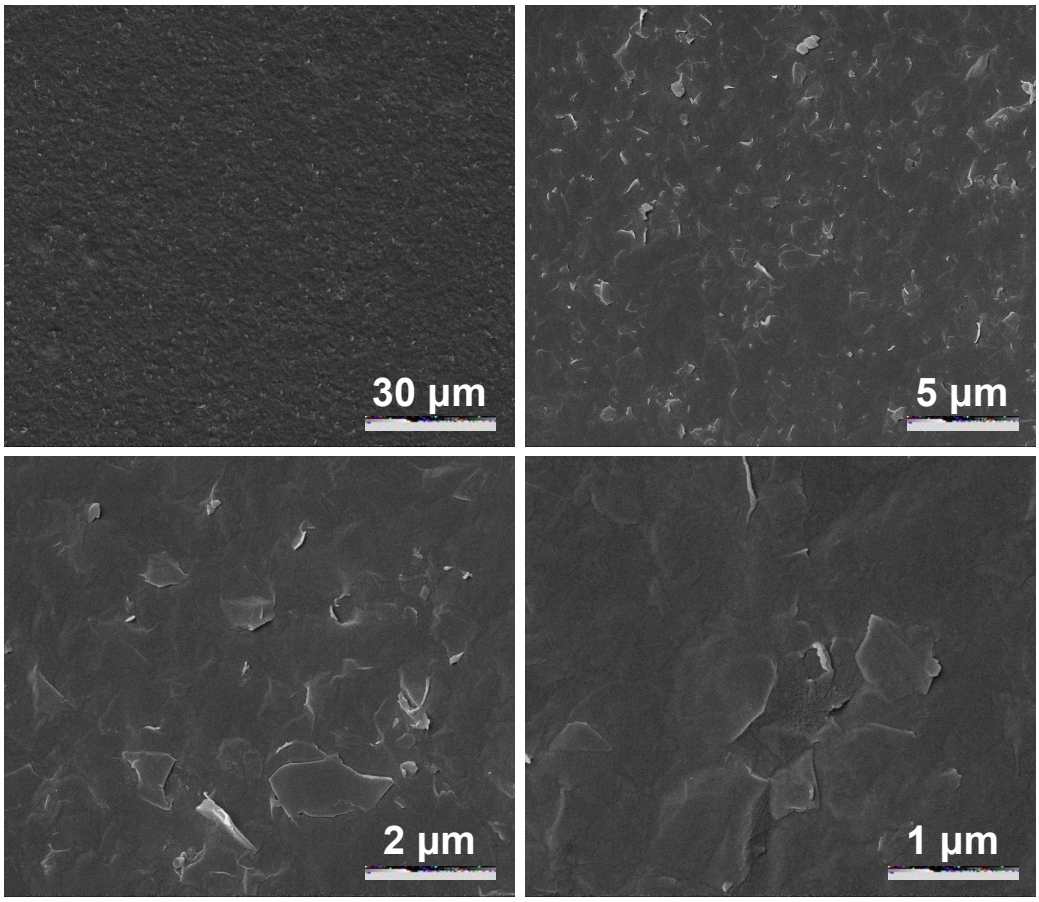

Fig. S22 Surface SEM images of vermiculite membranes after 100 dehydration-hydration cycles.

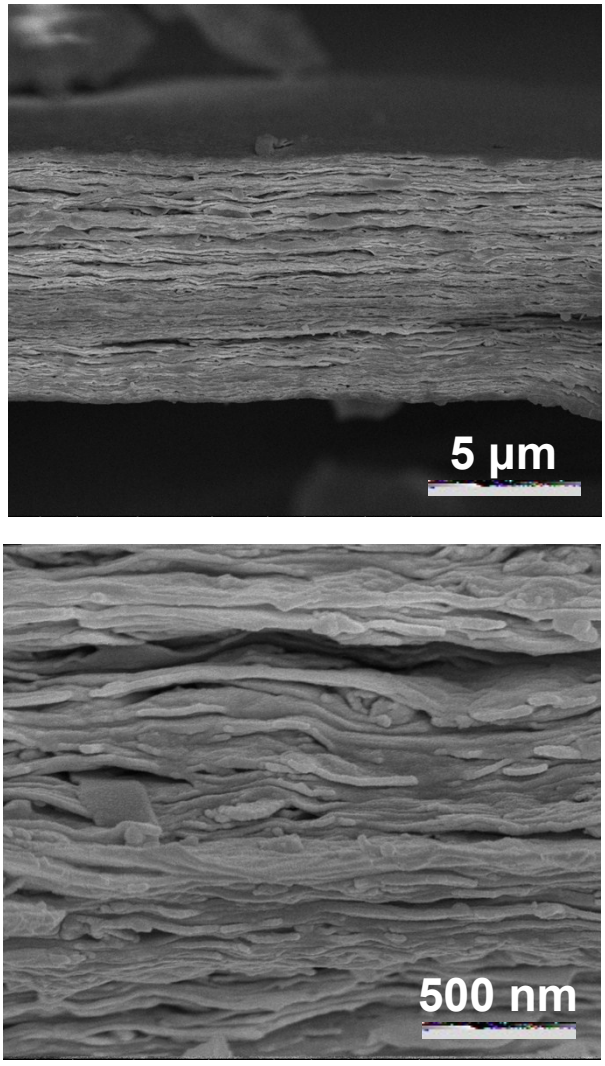

Fig. S23 Cross-section SEM images of vermiculite membranes after 100 dehydration-hydration cycles.

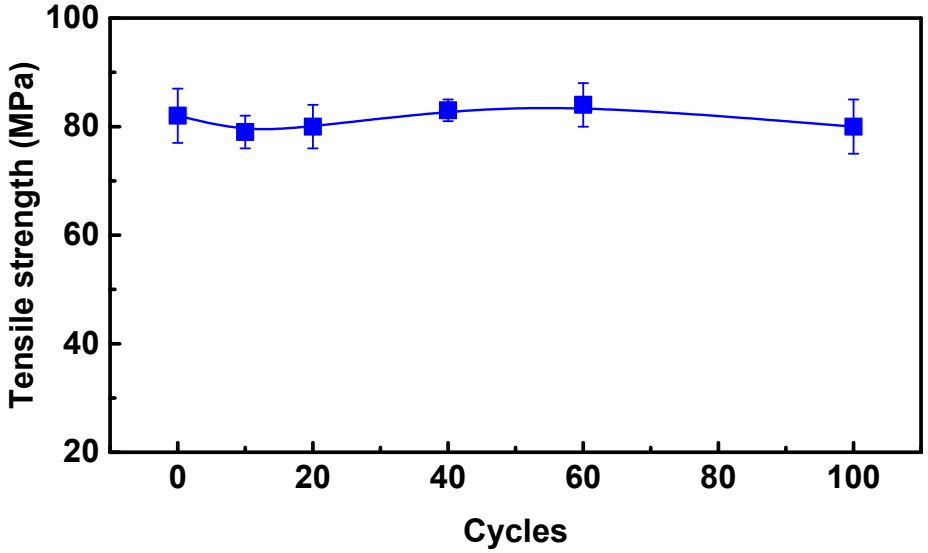

Fig. S24 Tensile strength of cross-linked vermiculite membranes during dehydration-hydration cycles.

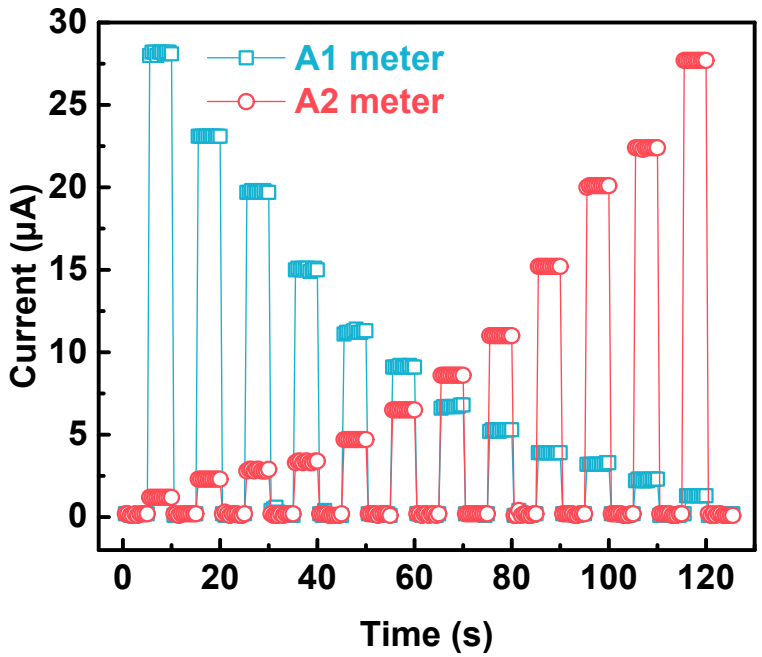

Fig. S25 The recorded current signals of A1 and A2 meters versus time.

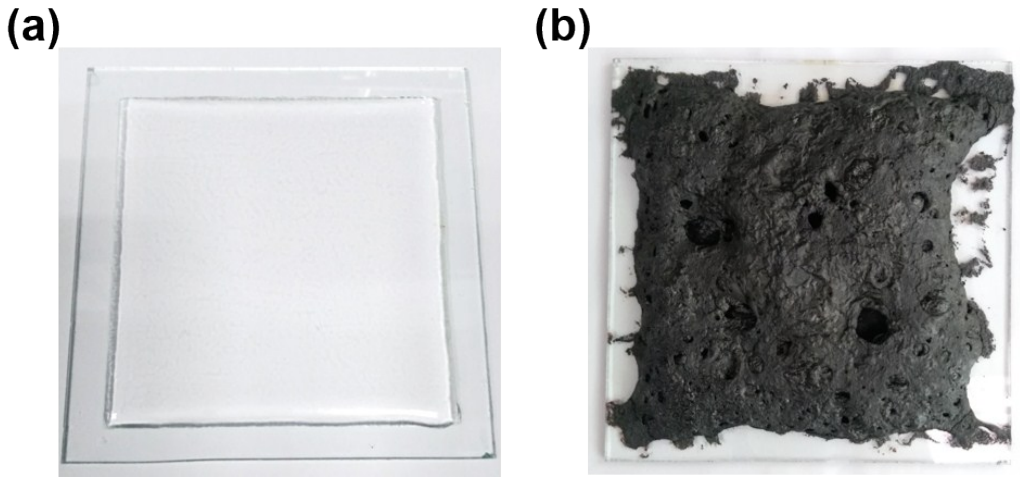

Fig. S26 Photos of conductive hydrogels: (a) initial conductive hydrogels, (b) conductive hydrogels after thermal annealing at 300 ^{o}C for 2h.

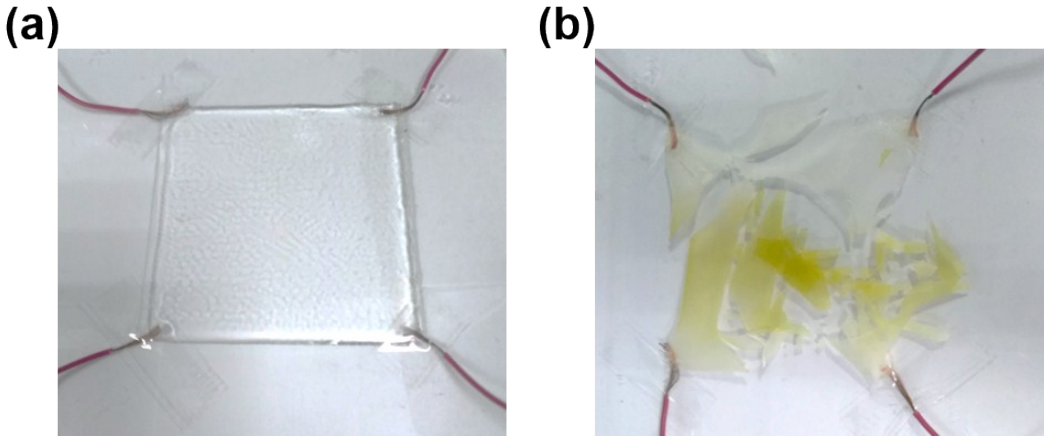

Fig. S27 Photos of conductive hydrogels: (a) initial conductive hydrogels, (b) conductive hydrogels after 3 dehydration-hydration tests.

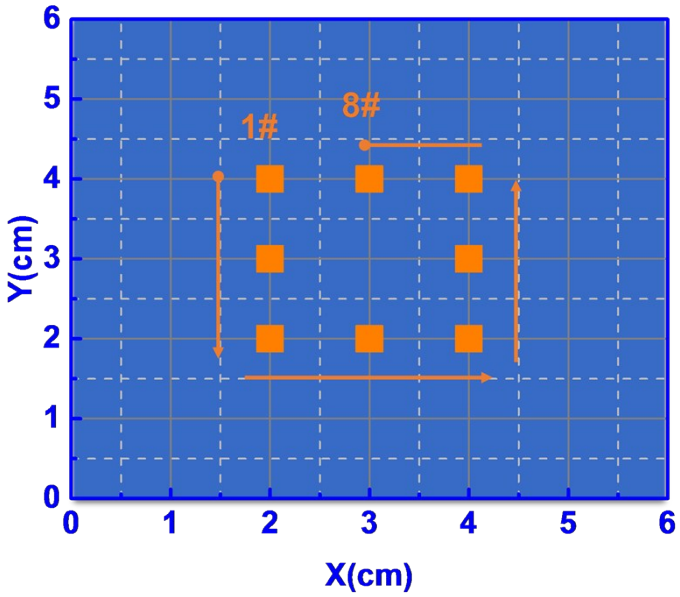

Fig. S28 Eight points from 1# to 8# were sequentially touched on the ionic touch panel to investigate the accuracy of position.

Table S1.

Comparison of ion conductivity and tensile strength of ion-conducting composite and vermiculite membranes.

Samples	Tensile strength (MPa)	Ion conductivity (S cm^{-1})	References
Co-PMPEG/LiTFSI	0.25	6×10^{-5}	S1
PVDF-co-HFP/EMIOTf	0.02	2×10^{-4}	S2
PMMA/$LiClO_4$	0.25	5×10^{-4}	S3
Wood-PAM/KCl	36	5×10^{-4}	S4
PAA/[C_2mim][$EtSO_4$]	0.01	2.2×10^{-3}	S5
PVA/LiCl	0.15	2×10^{-2}	S6
Zwitterionic gel/LiCl	0.05	2×10^{-2}	S7
PAMPS/[EMIm][DCA]	7.7	2.4×10^{-2}	S8
Polyampholyte/KCl	1.9	3×10^{-2}	S9
Vermiculite membranes	41	4.5×10^{-1}	This work
Cross-linked vermiculite membranes	83	4.5×10^{-1}	This work

References

1 L. Shi; T. Zhu; G. Gao; X. Zhang; W. Wei; W. Liu and S. Ding, *Nat. Commun.,* 2018, **9**, 2630.

2 Y. Cao; T. G. Morrissey; E. Acome; S. I. Allec; B. M. Wong; C. Keplinger and C. Wang, *Adv. Mater. ,* 2017, **29**, 1605099.

3 J. Wang; C. Yan; G. Cai; M. Cui; A. Lee-Sie Eh and P. See Lee, *Adv. Mater. ,* 2016, **28**, 4490-4496.

4 W. Kong; C. Wang; C. Jia; Y. Kuang; G. Pastel; C. Chen; G. Chen; S. He; H. Huang; J. Zhang; S. Wang and L. Hu, *Adv. Mater. ,* 2018, **30**, 1801934.

5 B. Chen; J. J. Lu; C. H. Yang; J. H. Yang; J. Zhou; Y. M. Chen and Z. Suo, *ACS Appl. Mat. Interfaces* 2014, **6**, 7840-7845.

6 Q. Rong; W. Lei; J. Huang and M. Liu, *Adv. Energy Mater.,* 2018, **8**, 1801967.

7 X. Peng; H. Liu; Q. Yin; J. Wu; P. Chen; G. Zhang; G. Liu; C. Wu and Y. Xie, *Nat. Commun.,* 2016, **7**, 11782.

8 Y. Ding; J. Zhang; L. Chang; X. Zhang; H. Liu and L. Jiang, *Adv. Mater. ,* 2017, **29**, 1704253.

9 T. Long; Y. Li; X. Fang and J. Sun, *Adv. Funct. Mater. ,* 2018, **28**, 1804416.